On the Optimization of Spread Spectrum Chirps Into Arbitrary Position and Width Pulse Signals. Application to Ultrasonic Sensors and Systems

A. RODRÍGUEZ-MARTÍNEZ[ID]**1, (Senior Member, IEEE), L. SVILAINIS**[ID]**2, (Senior Member, IEEE),**
M. A. DE LA CASA-LILLO[ID]**3, T. G. ALVAREZ-ARENAS**[ID]**4, (Senior Member, IEEE),**
A. ALEKSANDROVAS[ID]**2, A. CHAZIACHMETOVAS**[ID]**2,**
AND A. SALAZAR5**, (Member, IEEE)**

[1]Communications Engineering Department, University Miguel Hernandez of Elche, 03202 Elche, Spain
[2]Electronics Engineering Department, Kaunas University of Technology, 51368 Kaunas, Lithuania
[3]Bioengineering Institute, University Miguel Hernandez of Elche, 03202 Elche, Spain
[4]Institute for Physical and Information Technologies, Spanish National Research Council, 28006 Madrid, Spain
[5]Institute of Telecommunications and Multimedia Applications, Universitat Politècnica de València, 46022 Valencia, Spain

Corresponding author: A. Rodríguez-Martínez (arodriguezm@umh.es)

ABSTRACT This work presents in detail a new method for the optimization of rectangular spread spectrum excitation signals for its use in simple and low-cost ultrasonic pulsers, but that could be extended to other applications based on spread spectrum signals. Starting from rectangular linear frequency modulated (RLFM) chirps, it uses the transfer function of the transmitted signal and received echoes from reference specimens to iterate through a recursive algorithm to obtain arbitrary position and width pulse (APWP) signals with the desired bandwidth, maximizing the energy and the flatness of the spectrum, and enhancing the resolution and dynamic range of conventional chirp excitation signals. This optimization procedure can be repeated for any transducer and material, so that it achieves the best performance in each experimental environment. Such characteristics are ideal for Time-of-Flight estimation, imaging, and applications in which spectral regularity is needed, such as the Split Spectrum Processing (SSP) algorithm, which is used as example to test the performance of the proposed excitation signals. It also allows to specify and change the bandwidth reducing the need to change the transducers. The method is tested with different transducers (2 and 5 MHz focused transducers) and complex composite materials (aluminum-carbon aviation composite and high porosity GFRP composite) in immersion setup for imaging applications using SSP algorithm.

INDEX TERMS Ultrasound, spread spectrum, chirp, arbitrary position and width pulses, split spectrum processing, nondestructive testing.

I. INTRODUCTION

Ultrasonic nondestructive testing has been used in all areas of industry and research for many years, as it provides a wide range of applications and solutions for the characterization of the physical and mechanical properties of the materials, their inner composition, structural condition, aging behavior, etc [1], [2]. The number of environments and materials in which it can be used is endless, from gases to biological tissues, new complex nano-doped composites or large vessel hulls. The range of applications is also overwhelming, but almost all of them can be grouped, if

attending to their purpose, in three general groups of application: defect detection, characterization and imaging [3]–[6]. Finally, regarding the methodologies used, despite we would need a full book only to list the number of processing algorithms, procedures and methods used in ultrasound technologies, they can also be grouped in two sorts of methods, those based on time domain analysis and those based on frequency domain analysis, which combined lead to a third category for the methods that use both approximations combined [7], [8].

The methods based on time domain analysis are mainly devoted to calculate either the Time of Flight (ToF) between pulses and echoes coming from the irregularities (inhomogeneities) inside the material, which will be used to locate them or calculate propagation velocities, and/or the

The associate editor coordinating the review of this manuscript and approving it for publication was Wuliang Yin [ID].

difference in the amplitude between them, which will provide information about the attenuation suffered by the mechanical waves, and therefore of the properties of the material and/or the reflectors, as its size, geometry, acoustic contrast, etc. [9]–[13]. In both cases, both the signal-to-noise ratio (SNR) and the bandwidth of the signals are of most importance, as they limit the accuracy and resolution of the measurement. On the other hand, the methods based on frequency domain are usually focused in the analysis of the variation with frequency of parameters such as the phase velocity and frequency dependent attenuation [14], or in the resonant behavior of the spectrum due to the recursive echoes that appear in layered structures, which can be analyzed using resonant spectroscopy [15]. These parameters provide information about the properties of the material, and are also utterly dependent on the SNR and the bandwidth. Finally, time-to-frequency analysis, such as spectroscopy imaging [16] or Split Spectrum Processing (SSP) techniques [17], [18], [46], are also affected by the regularity and shape of the spectrum. As these methods usually are based on the comparison of how materials respond at different frequencies, it is essential to have signals with spectrum as wide as possible, so a wider range of wavelengths can interact with the material, and also as homogeneous (regular or flat) as possible so all wavelengths are excited with similar energy.

To summarize, regardless of the method used, there are three parameters that are crucial and should be carefully analyzed when using any ultrasonic method: the SNR, that should be as high as possible, the bandwidth, that should be as broad as possible and/or as constrained to the specified limits as possible, and the spectral regularity or flatness. There are three factors that affect these parameters: the electronics used, the electrical excitation signal and the ultrasonic transducer. In the electronics, the acquisition equipment and the amplifiers are affected by noise, bandwidth, input impedance and quantization. Regarding the transducers, the bandwidth is limited by their AC response, and even using electrical matching, composite piezomaterials or matching layers, the available frequency rage is narrow [10], [19]–[22]. Regarding the excitation signals, besides its amplitude, there are two factors to consider. On the one hand the excitation signal waveform and on the other how the excitation is produced.

Regarding the excitation waveform, the most commonly used are; spikes, pulse signals, which are usually short rectangular pulses, and burst signals, which consist on a series of periodic pulses tuned to a specific frequency. These signals are usually preferred because they are easy to generate and the results obtained with them are easy to interpret and process, but they are very limited in terms of energy and bandwidth [23]. Therefore, if our goal is to produce ultrasonic signals with high energy and wide bandwidth, the best option is to use spread spectrum (SS) signals [24]–[27], such as these based on arbitrary waveforms [28], [29], chirp (FM-CW, LFM) [24], [30], non-linear chirp (NLFM) [20], [31] and PSK sequences [32]. The use of SS signals offers significant advantages over conventional signals:

- They achieve a considerable improvement in the SNR by increasing the duration of the excitation signal, without negatively affecting (reducing) the signal bandwidth [33].
- The signals can be adapted (programmed) so that the spectrum acquires a certain form, while the spectrum of pulse and burst signals have a fixed form (sync) [30].
- An expansion of the width above the transducer pass band can be achieved, increasing the out-of-band energy [29].

SS signals also have disadvantages, mainly related to their length (duration), dynamic range, spectral flatness and programmability. As for its length, SS signals have to be long to gain energy, which reduces the axial resolution, enlarges the dead zone, and could lead to overlapping reflections even for widely spaced echoes [34]. On the other hand, the dynamic range in the image is directly related to the dynamic range of the lateral lobes, that is, the relationship between the amplitudes of the main lobe and the lateral lobe, and the SS signals have large lateral lobes in the correlation [23]. For example, PSKs are good in perpendicular exploration, but they have significant lateral lobes and their spectrum is fixed and very irregular in the pass band [35], [36]. Chirp, especially non-linear ones, achieve relatively flat spectra, but their correlation also presents very high levels in the lateral lobes [24]. The cause is at the beginning and end of the signal, where all frequencies are present. The dynamic range can be partially improved by weighting the signals (Hamming, Hann, Tukey), but this will negatively affect efficiency [37], and reduce resolution due to the widening of the resulting main lobe. On the other hand, the spectral programming of the chirp is complex: there is no direct solution, although approaches with some success have been used [31], [38], [39]. To achieve acceptable spectral equalization, amplitude modulated chirp (AM) [40] could also be used, although it consists of reducing energy and therefore SNR, but if combined with non-linear frequency modulation (AM-NLFM) [40], it is possible to obtain relatively flat spectra, with good SNR and with the desired shape.

Finally, there is another important issue that needs to be analyzed, since the type of signal is as important as the way it is generated. All the signals described above require arbitrary waveform signal generators, analog-digital converters and linear analog amplifiers, resulting in very expensive, costly and energy-inefficient equipment. On the contrary, rectangular signals are generated by simple switches, without the need for conversion, so binary excitation is more attractive and is widely used because: (i) it is simpler and the cost of the equipment is lower [41], [42], (ii) has higher efficiency, resulting in less temperature and longer battery life [43] and (iii) the size and weight of the equipment are lower, allowing portable equipment to be designed. Unfortunately, binary signals have certain disadvantages in the same direction as those we saw related to the type of excitation, that is, the irregularity of the spectrum, since chirp (unipolar or bipolar) signals add curly to the spectrum [44], and the lack
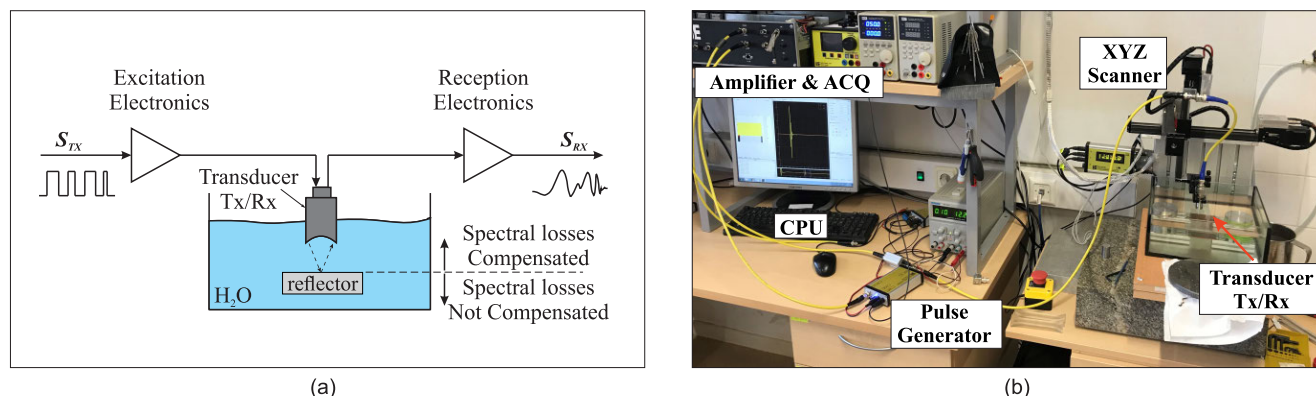
FIGURE 1. Experiment set-up (a) schematic and (b) experimental.

of dynamic margin, as additional lateral lobes appear in the correlation [29].

To overcome all the aforementioned limitations, we developed a new set of signals based on arbitrary position and width pulses (APWP) obtained from the conversion of NLFM-compensated signals to rectangular APWP prototypes followed by an iterative optimization process, which results in signals with flat spectrum, high SNR and programmable bandwidth. In [45] authors showed the performance of the optimization method by modelling, and a simple real example optimizing the signal passing through a Plexiglas delay line. The challenge remains now in analyzing whether these new set of excitation signals increase the performance of the processing methods in real measurement conditions analyzing noisy and complicated materials, such as complex composites, marble, grainy metallic alloys, etc. This paper explores one particular application, Split Spectrum Processing (SSP) algorithms, as it is a perfect candidate to benefit from the properties of the new signals.

The work is organized as follows. Section II explain in detail the optimization process of the APWP signals and reviews briefly the well known SSP algorithm designed to exploit it. Section III shows and discuss the results obtained with real samples of different sorts of materials, and finally we end up with the most relevant conclusions in section IV.

II. MATERIALS AND METHODS
A. MATERIALS AND EXPERIMENTAL SETUP
In order to perform the analysis, and following the general scheme shown in Fig. 1a, an immersion pulse-echo set-up was used (Fig. 1b), in which the transducer was mounted in a kinematic mount attached to a holder in a XYZ scanner used to scan the selected samples.

The scanner had a resolution of 200 μm per step in the XY axes and 100 μm in the Z axes. The pulser-receiver system was a SE-TX05-02 and the acquisition system a SE-AQ01-00, both from KTU Electronics [42], with 200 MHz sampling frequency in the pulser to generate the bipolar pulses, and 100 MHz sampling frequency

with 10 bits for the acquisition of the samples. Two set of transducers were used: a 2.25 MHz focused immersion transducer model IRZ602 from NDT Transducers LLC, and a 5 MHz focused immersion transducer model V309 from OLYMPUS. The liquid used was distilled water at 20° C. In all the measurements, once the sample was placed in its holder, the scanner was moved with the precision scanner in the Z axis so that the focal point of the transducer coincided with the surface of the sample, and then oriented using the kinematic mount to ensure normal incidence.

The materials to be analyzed were of different origins and properties: an experimental aluminum-carbon composite for aviation industry, and epoxy resin based GFRP of high porosity used for naval industry. For the optimization, reference blocks of aluminum 7075-T6 and standard epoxy were used. In all cases, the distance between the transducer and the sample -either the reference reflector or the sample under analysis-, was equal to the focal length of the corresponding transducer.

B. SPECTRAL OPTIMIZATION OF APWP SIGNALS
As stated in the introduction, the main idea is to use quasi chirp signals (sinusoids converted to rectangular waves) instead of AM-NLFM signals, as the efficiency and the exploitation of the dynamic output of the amplifier are much better than their sinusoidal counterparts. Unfortunately, the drawback is that the resulting spectral ripple in the band pass is much higher, which goes against our spectral flatness requirement. The alternative is to use the optimized APWP obtained using the approach showed in [45], in which an initial simple LFM chirp is converted to a NLFM-compensated chirp and then transformed into a rectangular APWP signal, which then feeds an optimization algorithm to compensate the spectral flatness.

We will summarize the steps followed to the derivation of the signals, so other researches can reproduce easily all the process. We encourage readers to review [45], where the derivation of the optimization algorithm and its theoretical justification is explained in detail. The equipment and
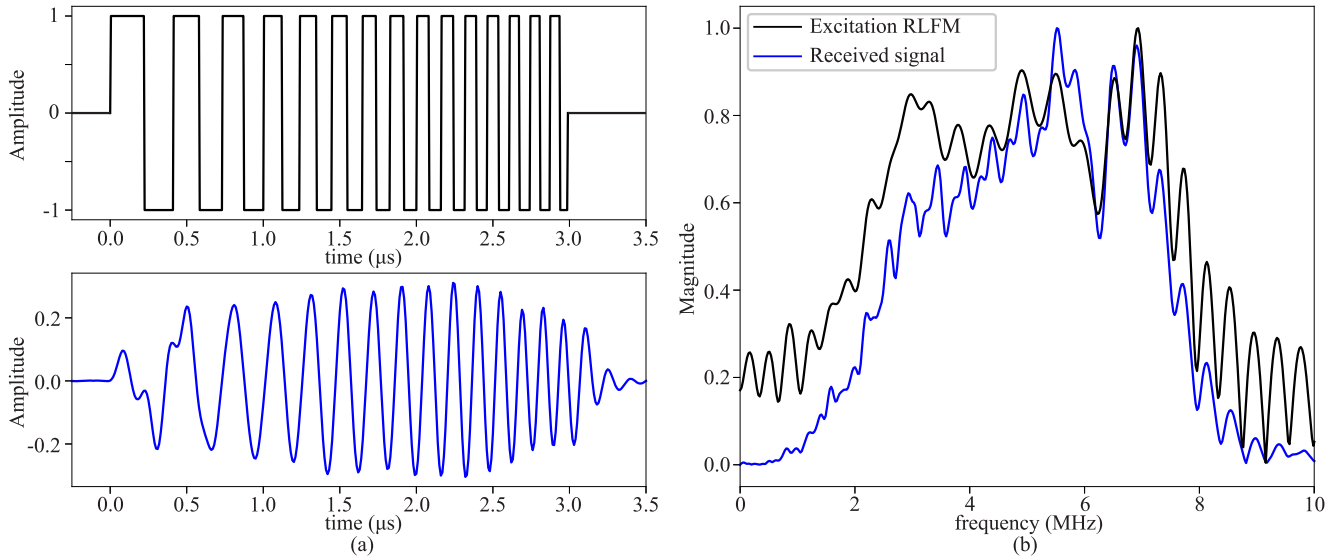
FIGURE 2. (a) Excitation RLFM chirp (up-black) and received signal (down-blue), and (b) corresponding normalized magnitude spectra in n.u.

materials used are described in the previous section, and in this particular example we will show the procedure for the optimization when the target is an aluminum block. Note that the optimization process is compensating the spectral loses of the excitation electronics, transducer frequency response, water-path and material surface, as depicted in Fig. 1a, so that the signal that penetrates into the material and interacts with it has the desired spectral properties. Once optimized, the resulting excitation signals can be used to analyze samples with similar properties (in this particular example, it would be aluminum-based specimens). If any of the parts of the set-up is changed, or we would like to analyze other sort of materials, the optimization process should be repeated.

In this example we will review the steps followed to optimize a 3 μs linear chirp with bandwidth 2-8 MHz to be used to analyze aluminum-based materials with a 5 MHz focused transducer, and selecting the desired resulting bandwidth also with the same limits (2-8 MHz), so the comparison will be more evident. The first step of the process will be to generate the rectangular quasi-chirp pulse to excite the transducer and record the received signal to analyze its spectrum. Fig. 2 shows the RLFM chirp used as excitation (Fig. 2a up-black), the received signal (Fig. 2a down-blue) and their respective magnitude spectrum (Fig 2b), where the aforementioned spectral ripples can be seen. Notice that signals have been normalized for its better comparison.

As aforementioned and described in [40], the easiest option to obtain the desired spectral shape, is to use a linear frequency modulated (LFM) chirp with the desired duration and bandwidth, convert it to its rectangular version (RLFM) as the one showed in Fig. 4a, and then use a compensation function to compensate the spectral losses, generating an amplitude modulated (AM) chirp: h

$$S_{AM}(f) = S_{RLFM}(f) \cdot \kappa(f), \qquad (1)$$

where $S_{RLFM}(f)$ is the frequency response of the transmitted rectangular LFM chirp, $S_{AM}(f)$ is the resulting frequency response of the compensated transmission signal, and $\kappa(f)$ is the compensation function calculated as:

$$\kappa(f) = \frac{|W(f))|}{\sqrt{|S_{RX}(f)|^2 + \alpha \cdot \max\left(|S_{RX}(f)|^2\right)}}, \qquad (2)$$

where $S_{RX}(f)$ is the spectrum of the received signal (Fig. 3a blue) when transmitting the RLFM signal (Fig. 3a black), $W(f)$ is a spectral windowing function used to control the bandwidth (Fig. 3a dotted grey), and α is a coefficient used for noise density approximation and to prevent $\kappa(f)$ from discontinuities, and is estimated by the signal to noise power densities ratio. Fig. 3b shows the resulting compensation function, and Fig. 3c the obtained compensated spectrum, whose inverse Fourier Transform will result in the desired AM chirp, shown normalized in Fig. 3d.

Now, as described in Chimura *et al.* [31], we can produce a NLFM chirp $s_{NLFM}(t)$ by nonlinear frequency modulation using the inverse function of the time-frequency characteristic $\tau(f')$ of the previous AM-compensated signal. According to Parseval's theorem, the energy of the AM-compensated signal $S_{TXAM}(f)$ and its nonlinear counterpart $s_{NLFM}(t)$ should be the same, and assuming that the spectrum in the frequency domain and the signal of constant amplitude in time domain are partially identical, the time-frequency relation $\tau(f')$ of $S_{TXAM}(f)$ (Fig. 4a) can be calculated as [31]:

$$\tau(f') = \int_0^{f'} |S_{AM}(f)|^2 \, \partial f, \qquad (3)$$

whose inverse function $f'(\tau)$ will be the instantaneous frequency function needed to generate the NLFM chirp. Unfortunately, $\tau(f')$ cannot be inverted because of its nonuniform gridding, therefore we will obtain $f'(\tau)$ (Fig. 4b)
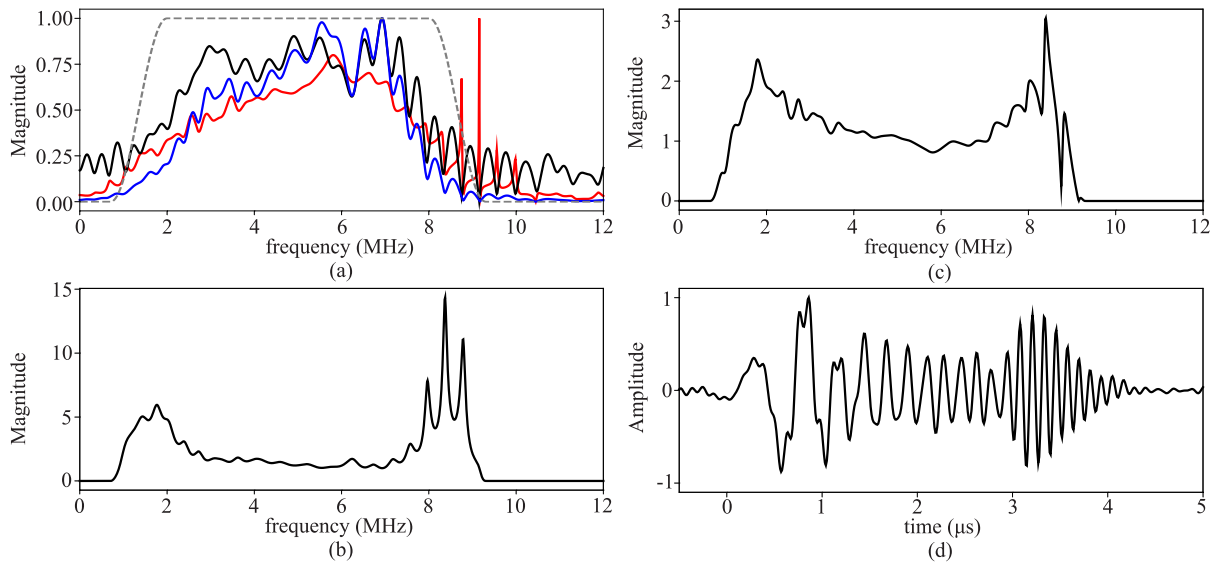
FIGURE 3. Normalized spectra of (a) excitation RLFM chirp (black), received signal (blue), transmission function (red) and spectral window (dotted-grey), (b) spectral compensation function $\kappa(f)$, (c) compensated spectrum $S_{AM}(f)$, and (d) resulting AM signal.
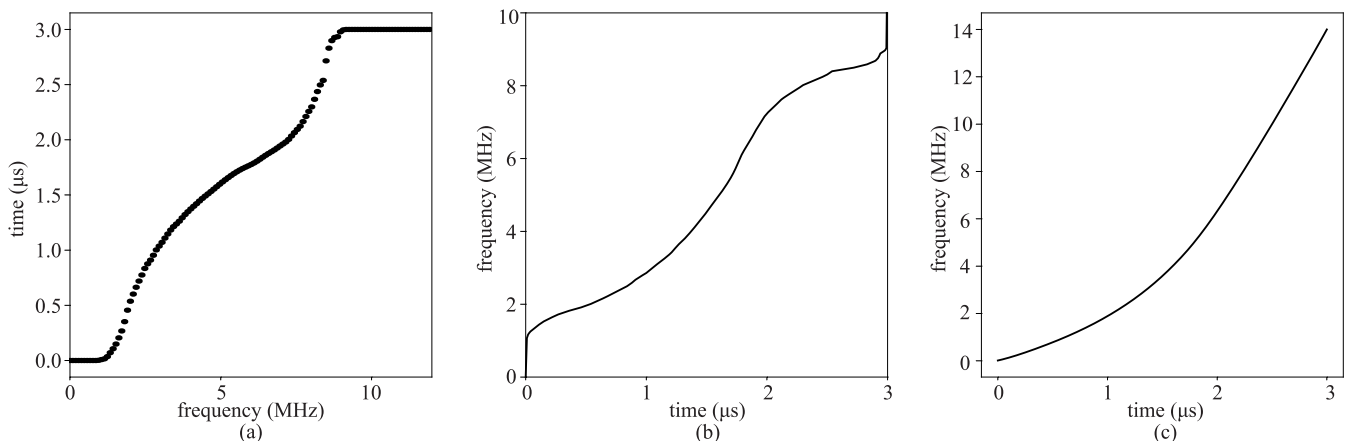
FIGURE 4. (a) Time-frequency characteristic function of the AM-compensated signal $S_{TXAM}(f)$, (b) interpolated instantaneous frequency function $f'(t)$, and (c) corresponding instantaneous phase function $\theta(t)$.

by linear interpolation:

$$\tau(f') \xrightarrow{lineal\ interp.} f'(\tau). \qquad (4)$$

Now, the phase function (Fig. 4c) can be obtained by integration:

$$\theta(t) = \int_0^t f'(t)\partial t, \qquad (5)$$

which will be used to produce the NLFM signal (red line in Fig. 5a) as:

$$s_{NLFM} = \sin(\theta(t)). \qquad (6)$$

Finally, the NLFM signal is converted to rectangular pulses to obtain $s_{RNLFM}(t)$ (black line in Fig. 5a), which will be the new excitation signal, considered as the seed APWP signal to feed the optimization process:

$$s_{RNLFM} = sign\{s_{NLFM}\}. \qquad (7)$$

Notice that both the spectrum of the transmitted RNLFM and its corresponding received signal (Fig. 5b) are highly lobulated, as can be seen in Fig. 5c, therefore we are still far from our goal. In order to achieve it, the optimization process will modify the seed APWP signal changing the width of the rectangular pulses recursively, aiming for the spectral flatness ξ in the bandwidth of interest. This spectral flatness will be estimated in each step as a measure of the standard deviation of the spectrum around its mean, accounting for its variability or flatness in the bandwidth, normalized by its mean value, accounting for the energy in the bandwidth, so the lesser ξ the better ratio flatness/energy. The flatness estimate at iteration $i - th$ will be calculated as:

$$\xi_i = \frac{\sqrt{\int_{f_{min}}^{f\,max} \left| |\overline{S_{RXi}(f)}| - |S_{RXi}(f)| \right|^2}}{|\overline{S_{RXi}(f)}|} \qquad (8)$$

where $|S_{RXi}(f)|$ is the magnitude spectrum of the received signal at the $i - th$ step and $\overline{|S_{RXi}(f)|}$ its mean.
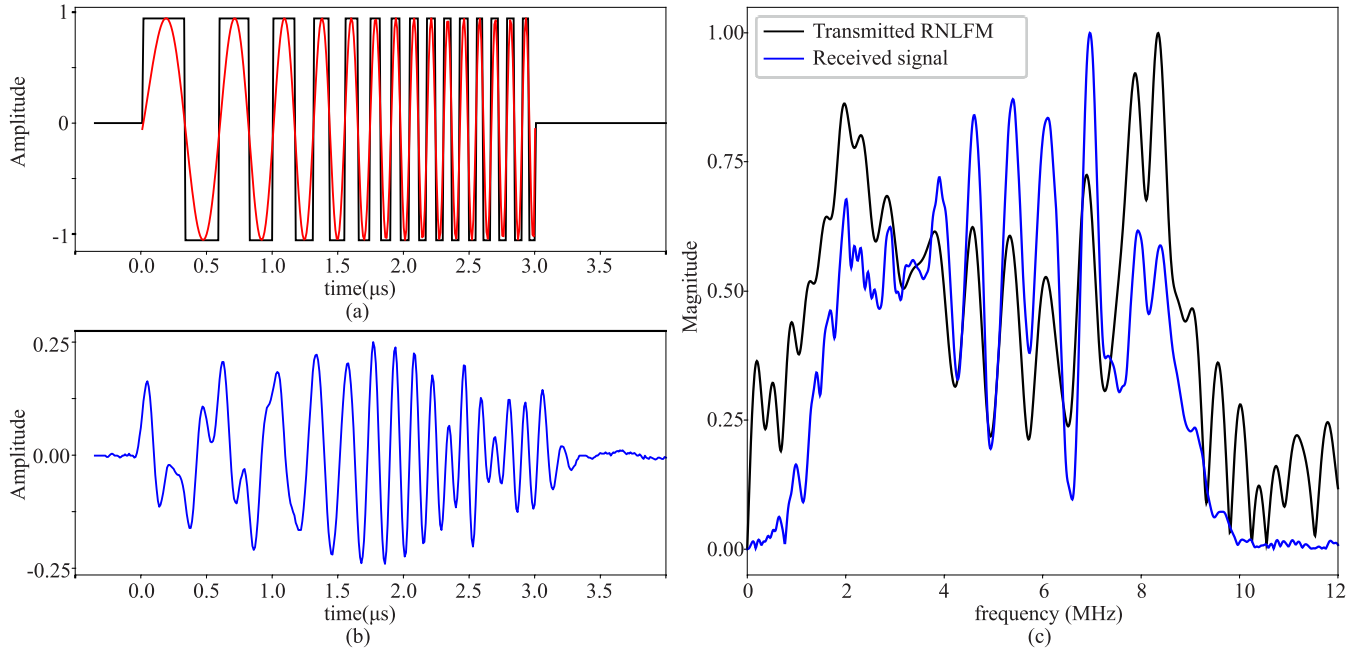
FIGURE 5. (a) Continuous (red) and rectangular (black) NLFM signals, (b) received signal when using the RNLFM (blue), and (c) their corresponding spectra normalized in n.u.
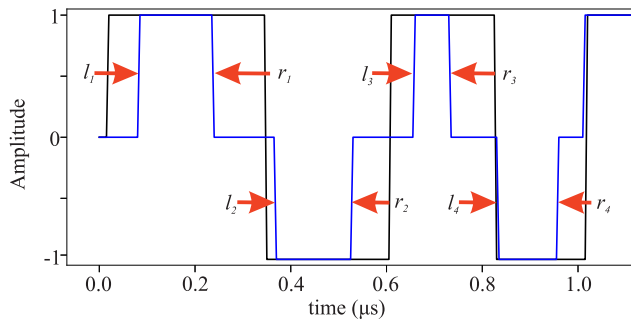

FIGURE 6. Example of width reduction at a particular iteration at step 2 of the optimization algorithm. RNLFM chirp seed (black), APWP prototype (blue), and red arrows that show the pulse reduction direction at stages 2 and 2b (left and right reduction respectively).

Therefore, once the optimization process converges, we will have the excitation signal that produces the flattest spectrum with the maximum possible energy. The optimization algorithm involves several levels with different loops. Any given original NLFM signal will have N rectangular pulses, each of them with length L_n samples, with $n = 1, \cdots, N$. There will be an optimization loop to optimize each pulse consecutively, and the process will be repeated until the spectral flatness parameter lays below certain threshold or there is no improvement. The whole process will follow the next steps:

1) Transmit the original rectangular NLFM signal obtained using (1)-(7) and calculate its initial spectral flatness estimate ξ_0. As aforementioned, this NLFM prototype will have N rectangular pulses, each of them with length L_n samples, with $n = 1, \cdots, N$;

2) Resize the $n - th$ pulse (starting from the first), transmit it and estimate the new spectral flatness ξ_{in}. Resizing involves a secondary recursive loop which is made shortening the pulses from the left side $l = 0, \cdots, L_{n-1}$, and the right side $r = 1, \cdots, l - 1$, (Fig. 6) both referring to number of samples;

   a) Transmit the resized pulse for a given l, and use the received signal to calculate its corresponding spectral flatness ξ_{inlr};

   b) Repeat (a) for $r = 1, \cdots, l - 1$;

   c) Choose the best candidate for the $n - th$ pulse using the one that provides the minimum ξ_{inlr}, and set $\xi_{in} = \min_{l,r} \xi_{inlr}$;

3) Fix the pulse $n - th$ to the one calculated previously and repeat 2 for the next pulse updating $n = n + 1$ until $n = N$;

4) Choose the best candidate for the new rectangular NLFM signal on the $i - th$ iteration as the one that provides the minimum spectral flatness ξ_{in}, and set $\xi_i = \min_n \xi_{in}$;

5) Repeat from 2 until the spectral flatness ξ_i lays below certain threshold or until there is no improvement in ξ_i, and choose as the optimum excitation signal the NLFM that has produced the minimum ξ_i.

Fig. 7 shows an example of the result obtained after the optimization of a 3 μs RLFM chirp with 2MHz-8MHz bandwidth, first converted to a RNLFM (black line) according to (1)-(7), into a APWP with the same bandwidth (blue line). A conventional 5 MHz pulse signal (red line) is included in the analysis to compare the advantages of using chirp signals. Notice that all the excitation signals are produced using
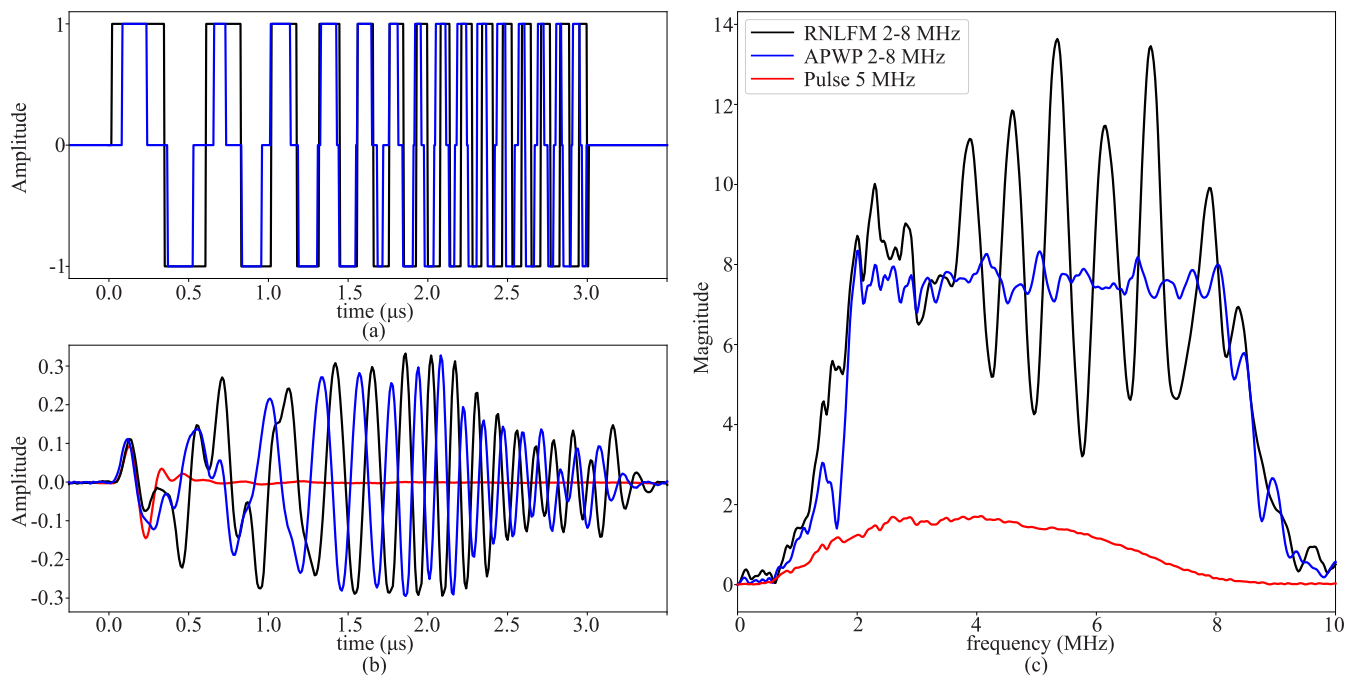
FIGURE 7. (a) RNLFM seed (black) and optimized APWP (blue), (b) received signals for RNLFM (black), APWP (blue) and conventional 5 MHz pulse (red), and (c) their corresponding spectra in n.u.
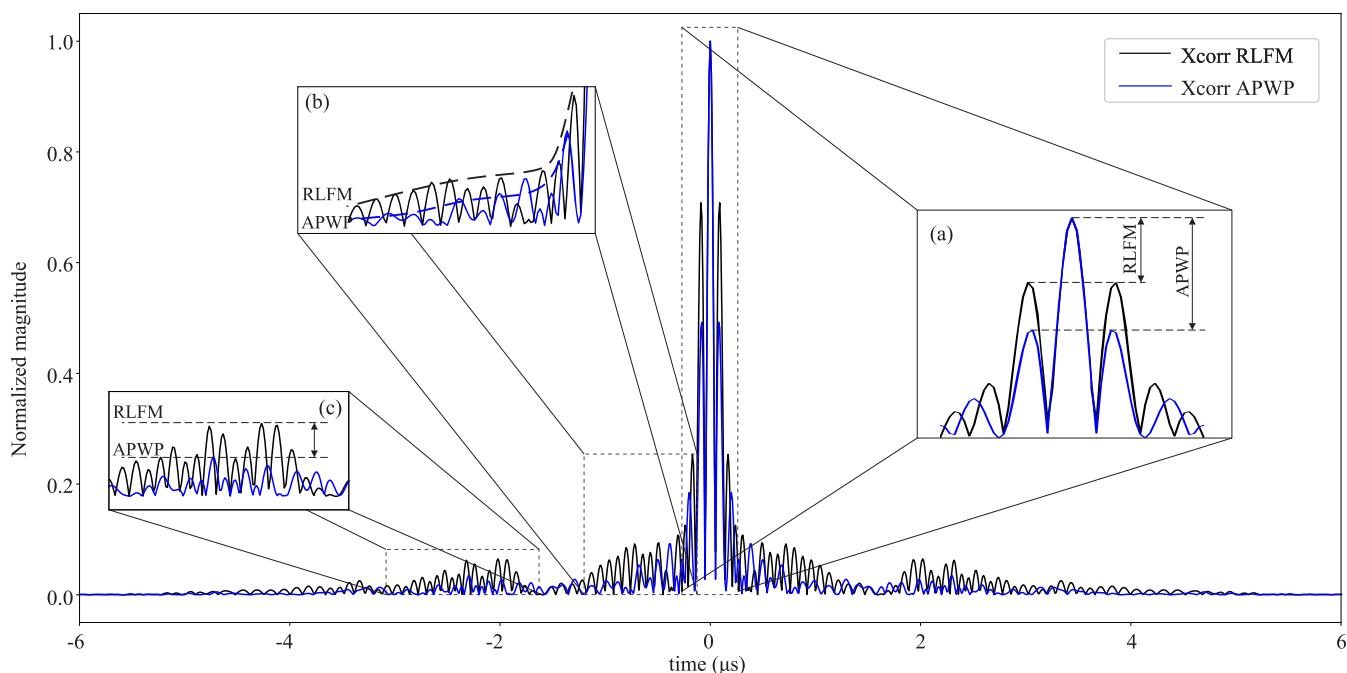

FIGURE 8. Cross-correlation function for the RLFM (black) and optimized APWP (blue) signals. Comparison of a) Main-to-Secondary lobe level, b) side lobes energy leakage, and c) width and height of lateral lobes.

rectangular pulses with the same excitation voltage. Fig. 7a shows the transmitted pulses, Fig. 7b the respective echoes coming from the aluminum test specimen for which the APWP was optimized, and Fig. 7c shows their spectra, where we can see how the spectral ripples have been significantly reduced, with the drawback of a significant energy reduction,

but the algorithm ensures that the resulting excitation signal has the maximum possible energy with the flattest spectrum. This figure shows clearly the performance of the optimization method, as the resulting APWP signal has a much more efficient use of the bandwidth than the conventional RLFM, specially considering the need of regularity (flatness) in the
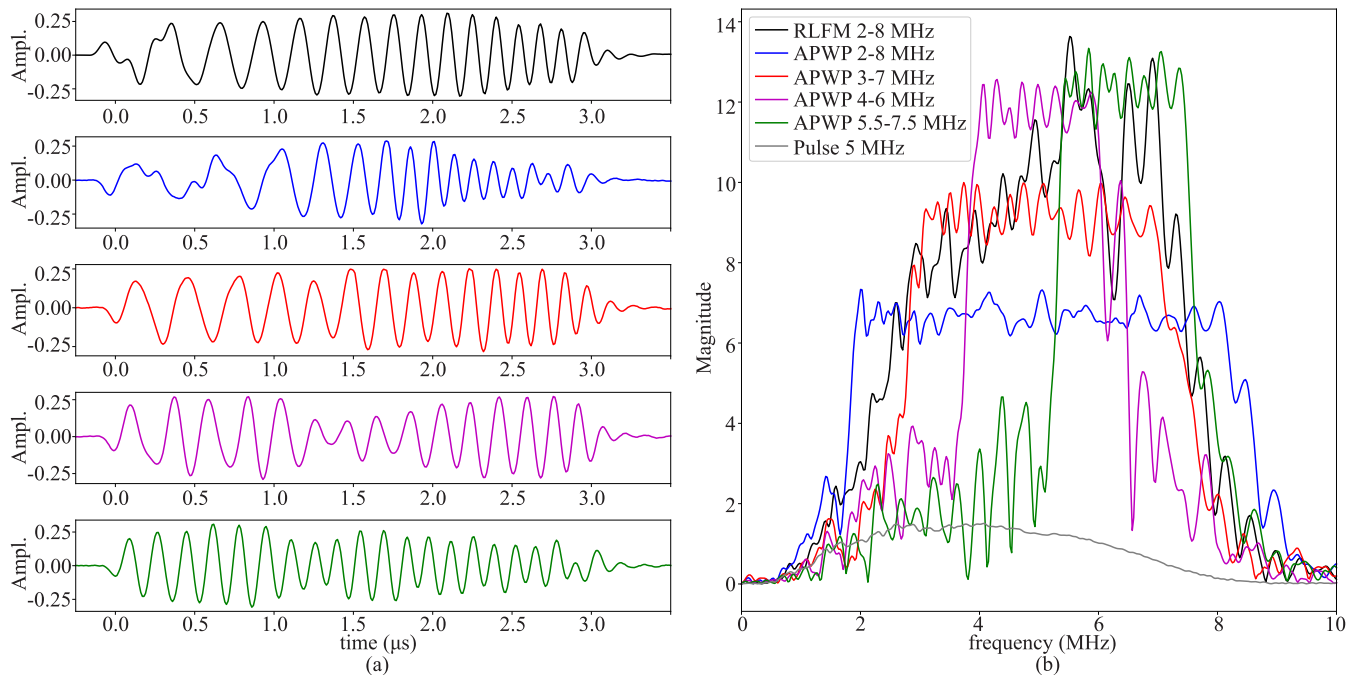
FIGURE 9. Example of APWP bandwidth programming using the optimization process. Signals in (a) time and (b) corresponding magnitude spectrum in n.u.

spectrum. Furthermore, despite the reduction in the energy supplied, it is still much higher and efficient than the conventional pulse.

Another significant advantage of the optimized signal is the improvement achieved in the cross correlation function, which is crucial for the estimation of the Time of Flight [45] and for its denoising performance when used as adapted filter. Fig. 8 shows the normalized auto-correlation of the conventional RLFM (black) and the optimized APWP (blue). As can be seen (insert (a) in Fig. 8), the Main-to-Secondary level achieved is significantly higher for the new APWP compared to the RLFM. The energy leakage due to side lobes is also much lower(insert (b) in Fig. 8). Finally, the width and height of the lateral lobes (insert (c) in Fig. 8) is also much smaller for the optimized APWP than for the conventional RLFM. All these improvements redound in the performance of the of the system in terms of its resolution and imaging, as we will see in the results.

Finally, as an additional feature of the algorithm, the bandwidth of the resulting signal can be programmed adjusting the bandwidth of interest in the optimization process, therefore the same transducer can be used to produce very specific spectral shapes, achieving in all cases the flattest and more energetic signal possible. This is illustrated in Fig. 9, which shows APWP signals of different bandwidth optimized for aluminum, all of them produced with the same transducer in the same experimental set-up, the same RLFM seed, and the same excitation voltage. See legend in Fig. 9b for the selected bandwidths. The spectrum of the conventional 5 MHz pulse produced with the same set-up and voltage is included for comparison.

C. SPLIT SPECTRUM PROCESSING ALGORITHM

Split spectrum processing (SSP) is a well-known technique in the field of ultrasound used to reduce the grain noise [17], [18], [46], but also used in other areas as [47]–[49], due to its simplicity and the good results that it provides. This algorithm exploits the assumption that the reflection of small scatterers inside the material are frequency sensitive due to the random distribution of the phases received from every one of them, as they depend on the size and orientation of the scatterers. On the other hand, defects of size enough will reflect a significant number of wavelengths with the same phase (Fig. 10a and 10b)

The basic idea of the SSP algorithm is to pass the received signal through a bank of filters covering the bandwidth of the transmitted pulse, and compare the outputs of the filters using a nonlinear recombination (Fig. 10c), so that when all the outputs are similar, the resulting output is enhanced (defect), and decreased when they are different (grain noise). Note that according to this idea, we would like to have signals with wide bandwidth, high SNR and with a spectrum as regular (flat) as possible so all the wavelengths are excited similarly and therefore the nonlinear comparison between bands is fair. Now it is clear why the proposed optimized APWP signals may be of interest to this algorithm, in order to make it a bit more efficient and reliable.

Regarding the specific design of the algorithm, there are many parameters to consider. On the one hand, considering the design of the filter bank, we have to choose the number of bands, the bandwidth of each band, the overlap between bands and the filters design. These parameters have been deeply studied in previous works of the authors [17], and the
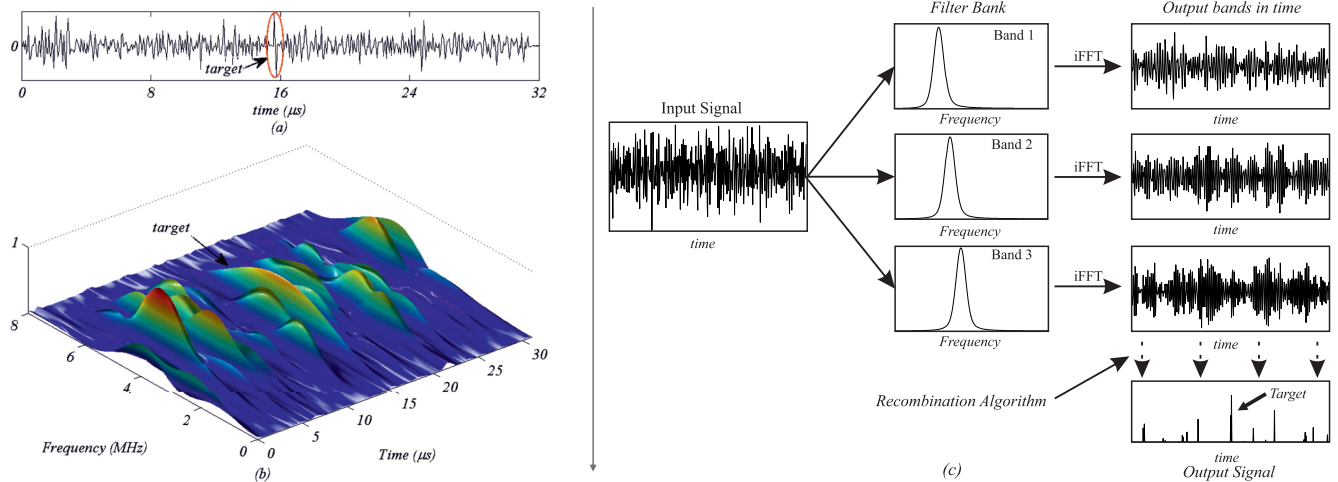
FIGURE 10. Example of application of SSP algorithm (a) Ultrasonic signal in time domain, (b) corresponding spectrogram, (c) general schematics for the SSP algorithm.

best results have been achieved using Gaussian filters equally distributed along the operational bandwidth and with 50% of overlap. The impulse response of the Gaussian filters can be calculated using:

$$h_i(t) = e^{-t^2/2\sigma_i^2} \cos(2\pi F_{Ci} t), \qquad (9)$$

where F_{Ci} is the central frequency of the $i-th$ band and σ_i^2 the variance of its corresponding Gaussian window, defined as:

$$\sigma_i^2 = \frac{\sqrt{\ln 2}}{2\pi B_i F_{Ci}}, \qquad (10)$$

where B_i is the relative bandwidth at 3dB of the corresponding filter:

$$B_i = \frac{\Delta B \cdot (1 + 2R_{ol})}{L}, \qquad (11)$$

with ΔB the bandwidth of analysis, R_{ol} the filters overlap factor, in this case 0.5, and L the number of bands of the filter bank.

The number of bands is a very sensitive parameter, as it directly affects the probabilities of detection (PD) and false alarm (PFA). A high number of bands ensure that only real defects of enough size will produce similar outputs in all the bands and therefore reduce the probability of false alarm, but smaller, deeper or misaligned defects will not be detected. On the other hand, reduced number of bands will increase the probability of false alarm.

Regarding the recombination methods, according to our experience and the preliminary analysis performed on the materials, the polarity thresholding recombination algorithm will be used as the basis for the recombination as it produces the most reliable results in this case. According to this algorithm, when all the bands have the same phase (sign of the samples in time domain), the output will be the value of the original signal, and zero otherwise. For a given signal $x[n]$,

considering $x_i[n]$ as the output of the corresponding filter $h_i[n]$, that is, $x_i[n] = x[n] * h_i[n]$, the result of the recombination $y[n]$ will be:

$$y[n] = \begin{cases} x[n] & x_i[n] < 0 \ \forall n \ or \ x_i[n] > 0 \ \forall n \\ 0 & otherwise \end{cases} \qquad (12)$$

This results in a very restrictive condition, which is very conservative for high dispersive materials, so we will use a less restrictive version in which the output is scaled with a factor proportional to the number of bands with the same polarity. The scaling factor M will be calculated as:

$$M = \frac{|L_+ - L_-|}{L}, \qquad (13)$$

with L_+ and L_- the number of positive and negatives values respectively for each n.

Finally, in case of highly dispersive materials, pruning technique [17] can be also applied to eliminate the bands more affected by dispersion or gain noise.

III. RESULTS AND DISCUSSION
In this section we will show the results after processing some materials using Split Spectrum Processing algorithms with the optimized APWP signals. We will start by showing the results of the optimizing process with different configurations, and then the results of the processing stage.

A. OPTIMIZATION OF APWP SIGNALS
As stated in section 2.1., we used two sorts of transducers, of 2 and 5 MHz, focused in both cases. We will use RLFM chirp pulses of 3 μs for both transducers and excitations, because this duration offer a good compromise between energy and axial resolution for the selected specimens. For the 2MHz transducer, the bandwidth of the RLFM pulses will be of 2 MHz, in the band from 1 MHz to 3 MHz, and for the 5 MHz transducer it will be of 6 MHz, in the band
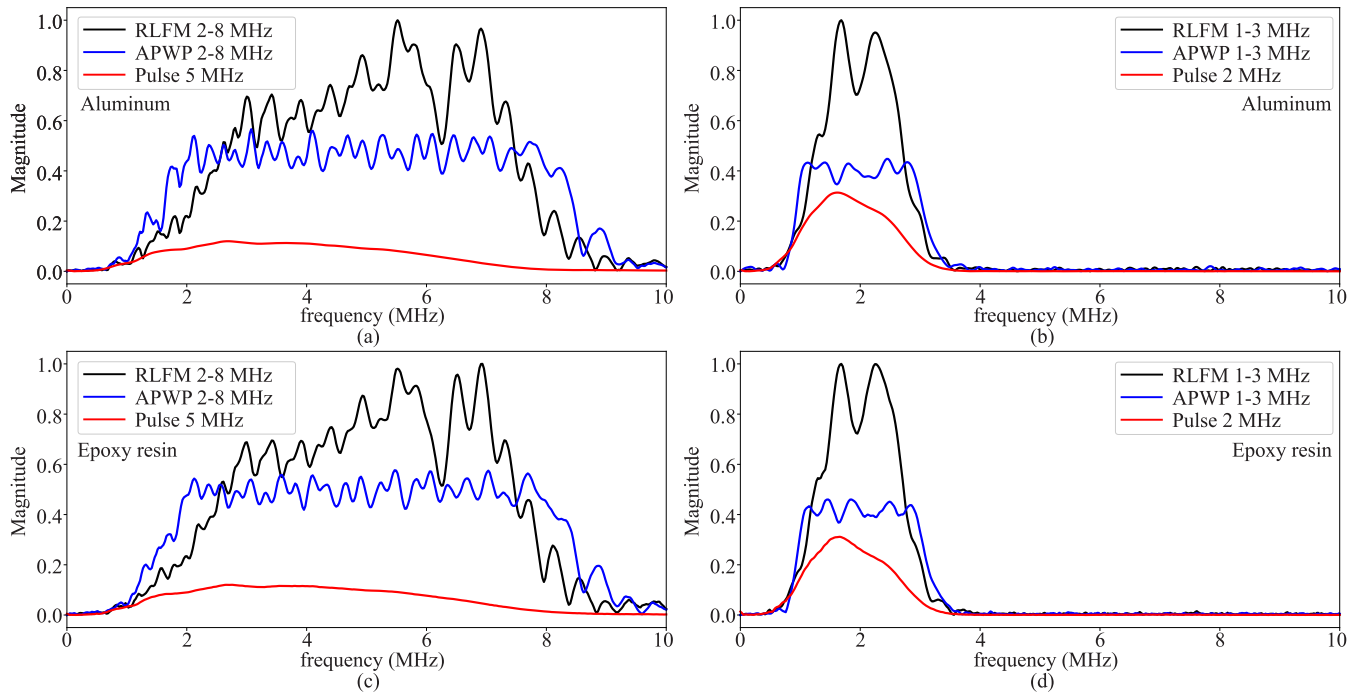
FIGURE 11. Normalized spectrum in n.u. for RLFM (black), optimized APWP (blue) and pulse (red) excitations (a) 5 MHz transducer on aluminum specimen, (b) 2 MHz transducer on aluminum specimen, (c) 5 MHz transducer on Epoxy resin specimen and (d) 2 MHz transducer on Epoxy resin specimen.

from 2 MHz to 8 MHz. In both cases, the optimized APWP are designed to operate in the same bandwidth as the original RLFM pulses, that is, 1 to 3 MHz in the 2 MHz transducer, and 2 to 8 MHz for the 5 MHz transducer. These SS signals will be compared with conventional pulse excitation signals centered at the corresponding transducer's central frequency.

The APWP signals were optimized for two different scenarios using reference specimens, depending on the material to be analyzed, aluminum or epoxy-based composites. Fig. 11 shows the resulting spectra after optimization for the four different scenarios; left figures for the 5 MHz transducer, right figures for the 2 MHz transducer, upper figures for the aluminum specimen, and lower figures for the epoxy resin specimen. In each case, signals were normalized respect to the RLFM chirp, which is the most energetic, but the excitation voltages were the same for all excitations in each experiment. As can be seen, in all cases the optimization algorithm achieve the expected objectives, that is, a very efficient use of the spectrum (flat pseudo-regular spectrum and wide bandwidth), and retaining the advantage of working with a long chirp, which ensures the best performance for the cross correlation function in detection and ToF estimation applications.

B. SPLIT SPECTRUM PROCESSING

We will see two examples to illustrate the behavior of the optimized APWP excitation compared to the conventional RLFM Chirp when combined with the SSP algorithm for denoising and imaging. In the first case, we analyze a very

complex matrix aviation composite specimen build up by layers of aluminum-6082 with 43% volume fraction of low modulus long carbon fibre reinforcements in a [0°, 90°] lay-up. The thickness of the flat-bottomed plate is 12 mm, and four holes of 4 mm, 6 mm, 8 mm and 10 mm were made on the specimen to analyse the imaging performance of each signal. An image of the actual plate and of its inner structure obtained by X ray analysis is shown in Fig. 12. For each excitation, a B-scan was acquired from the flat-bottom surface of the specimen along one axis passing across the holes (black dotted line in Fig. 12b and 12c), using a precision scanner with steps of 0.2 mm.

For this specimen, transducers and excitation signals are the same as in the first example of previous sections, that is, using a 5 MHz focused transducer, rectangular LFM chirps from 2 to 8 MHz and corresponding APWP signals optimized using the aluminum reference block. In all cases, signals were cross correlated with its corresponding reference before processing to reduce noise and compress the signal. The SSP algorithm was then applied using the scaled polarity thresholding recombination method and pruning the higher bands, so that only 5 bands from 1 to 3 MHz were considered.

Fig. 13 shows the results obtained, in which, for a better appreciation of the details, each Bscan is accompanied with a Ascan from an specific position (around 36 mm in the scanning direction marked with a black solid line in the corresponding Bscan) and displayed immediately below it. Upper figures (Fig. 13a, 13b and 13c) show the result for the RLFM chirp and lower figures (Fig. 13d, 13e and 13f)
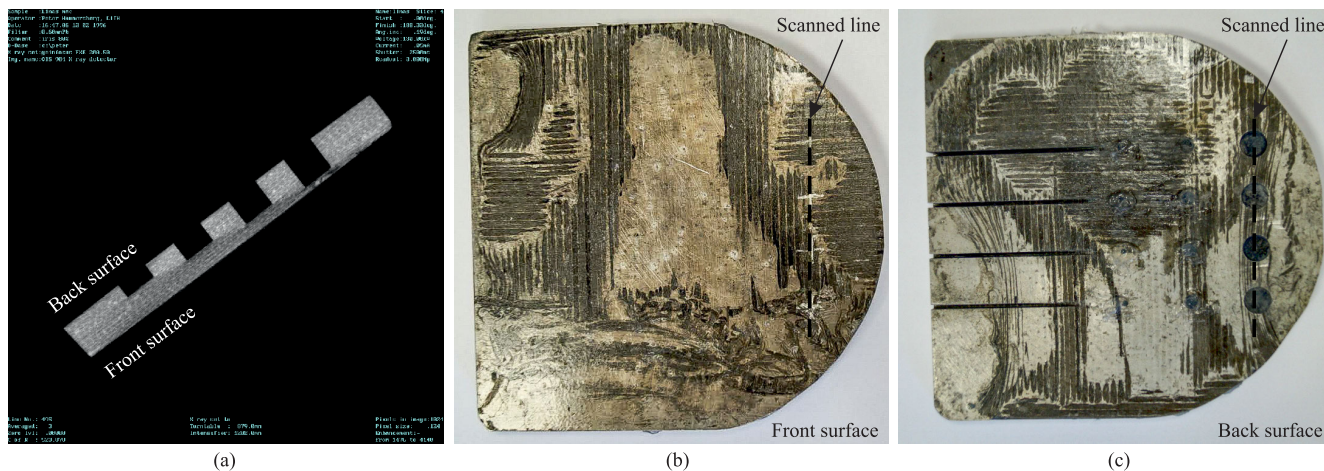
FIGURE 12. Aluminum-Carbon aviation composite. (a) XRAY image, (b) front (flat) surface and (c) back (machined) surface.
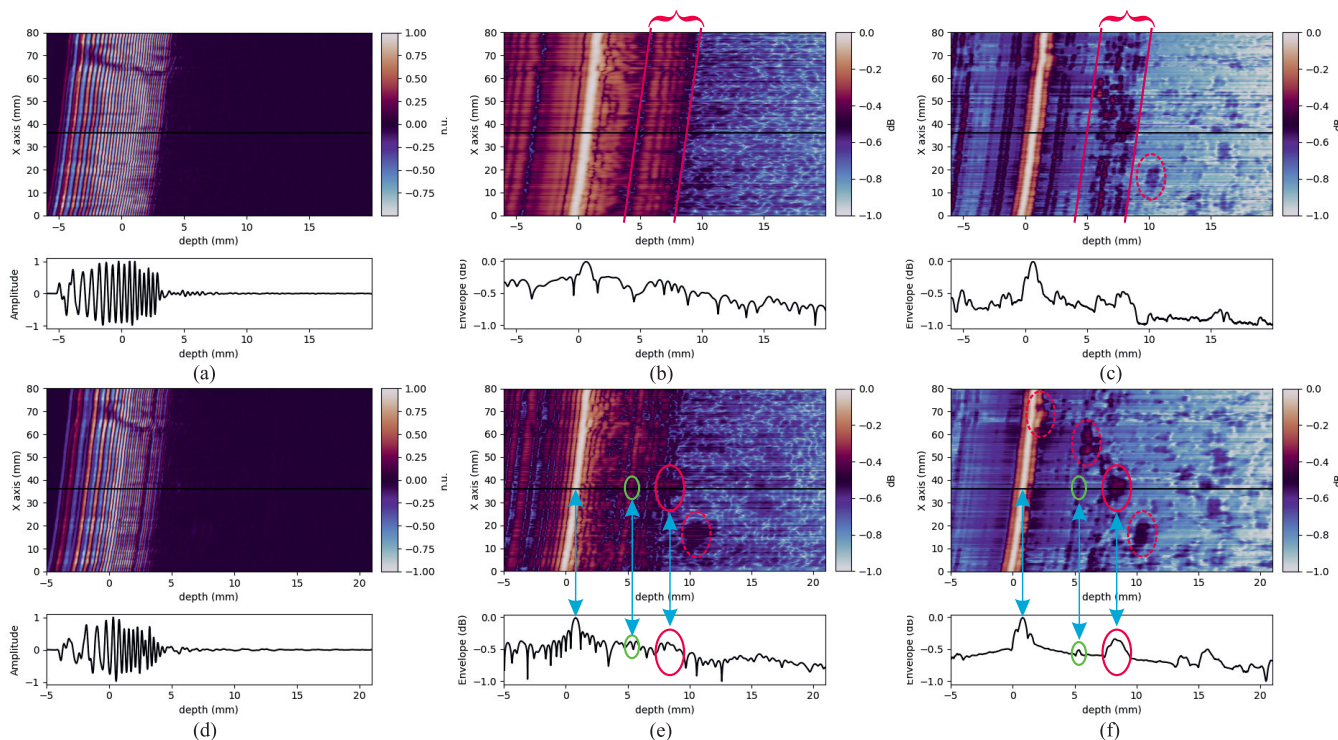

FIGURE 13. Results for the carbon-aluminum composite with the 5 MHz transducer. In each subfigure, upper graphic shows the Bscan and lower grahphic a Ascan at a particular position (horizontal black line in Bscans). (a) raw signal for RLFM, (b) compressed signal before SSP for RLFM, (c) result after SSP for RLFM, (d) raw signal for APWP, (e) compressed signal before SSP for APWP, (f) result after SSP for APWP.

for the optimized APWP. From left to right, it shows the raw unprocessed signals (Fig. 13a and 13d, amplitude in natural units), signals after compression with the references (Fig 13b and 13e, envelope in dB), and finally the result after applying the SSP algorithm (Fig. 13c and 13f, envelope in dB).

As it was expected, in both cases raw signals are not able to provide any information about the inner structure because of the grain noise and attenuation (Fig. 13a and 13d). Once

the compression is made, the strong lateral lobulation of the cross correlation function is clearly evident for the RLFM in Fig. 14b (area between the red lines), masking completely the echoes coming from holes in that region. On the other hand, the lateral lobes are significantly smaller for the new APWP signal (green ellipse), as can be seen in Fig. 14e and 14f, where only a small lobe remains. Notice that now echoes from holes 4 and 6 mm depth can be seen (red ellipses). Finally, after SSP, it is again clear the advantages of using the
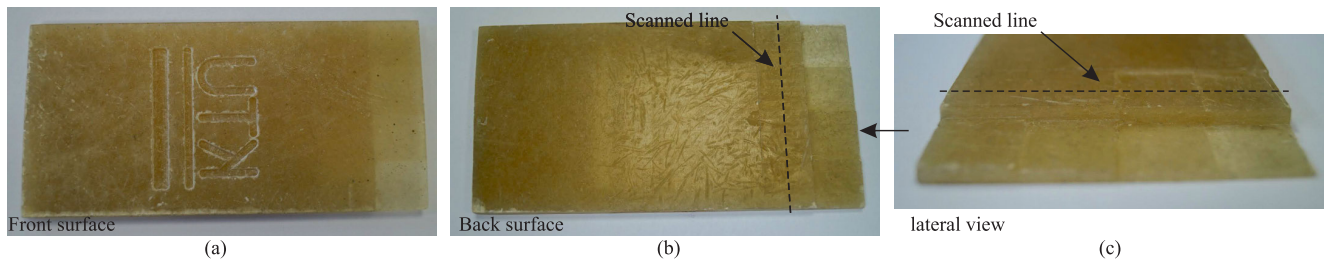
FIGURE 14. Porous epoxy GFRP naval composite. (a) front (flat) surface, (b) back (machined) surface and (c) lateral view.
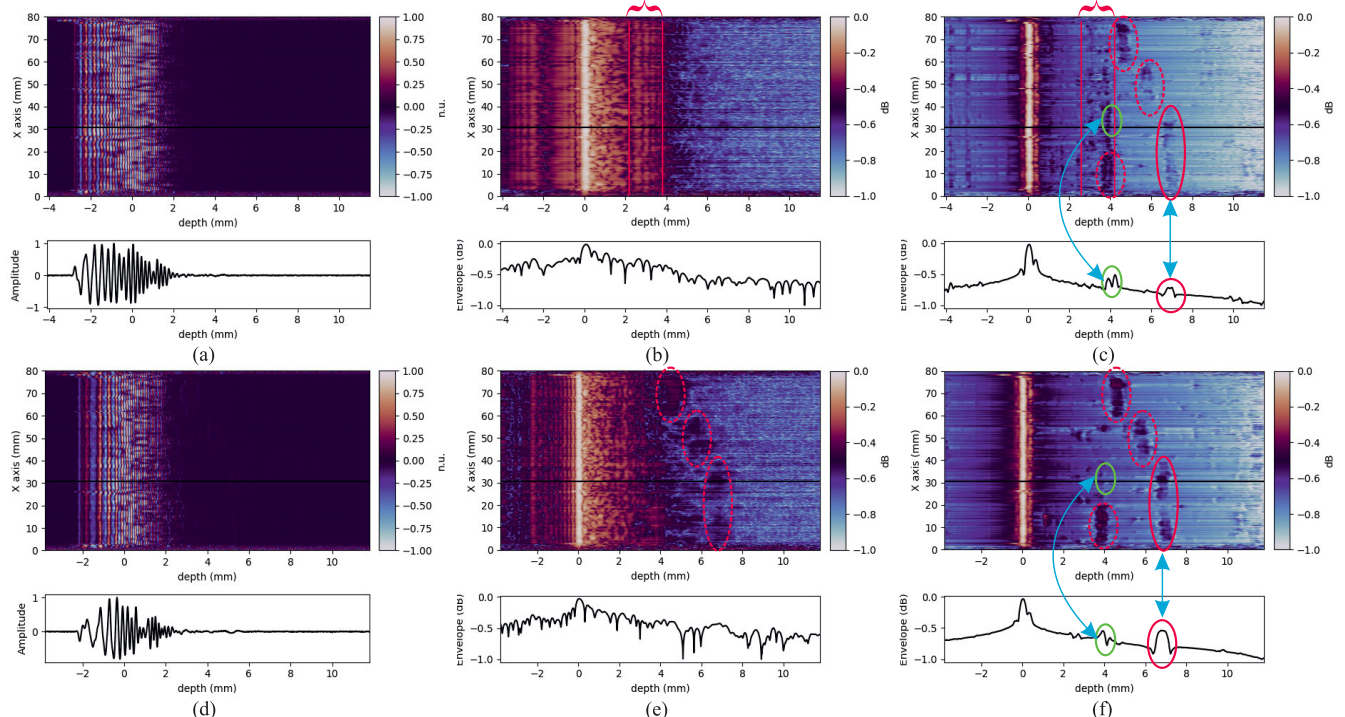

FIGURE 15. Results for the porous GFRP composite with the 5 MHz transducer. In each subfigure, upper graphic shows the Bscan and lower grahphic a Ascan at a particular position (horizontal black line in Bscans). (a) raw signal for RLFM, (b) compressed signal before SSP for RLFM, (c) result after SSP for RLFM, (d) raw signal for APWP, (e) compressed signal before SSP for APWP, (f) result after SSP for APWP.

optimized APWP signal, in the sense that all echoes in the lateral lobes' region can be seen (6 and 8 mm), and even the closer hole (10 mm) can be slightly appreciated because of the better dynamic range of the main-to-secondary lobe ratio, which also improves slightly the axial resolution. Note that the response of the SSP is also better for the APWP in therms of SNR, as can be clearly seen if we compare the Ascans in Fig. 13c and Fig. 13f.

In the second example, a high porosity GFRP composite made up of randomly oriented chipped glass fibers was analyzed, with the same transducer and signals optimized for epoxy composites. This sample has one flat surface and the other one has different thicknesses. An image of the actual plate is shown in Fig. 14. For each excitation, a B-scan was acquired from the flat-bottom surface of the specimen along one axis passing across the thick steps machined on the other surface (black dotted line in Fig. 14b and 14c), using the precision scanner also with steps of 0.2 mm. In this case, before

processing, signals were aligned for a better interpretation of the images.

This example shows again the superior performance of the APWP signals in terms of dynamic range, as even before SSP, the back surface echoes can be seen (Fig. 15e) in the compressed signals, while the poor dynamic range of the RLFM chirp masks all reflections (Fig. 15b). Notice that even after SSP, the secondary lobes persist for the RLFM, masking the delamination (Fig. 15c) that can be clearly seen when using APWP (Fig. 15f), where a better dynamic range and image resolution can be appreciated for all the echoes.

IV. CONCLUSION

In this work we showed a method for the optimization of rectangular LFM chirps into APWP signals in terms of bandwidth efficiency and regularity (flatness), and cross correlation function performance. We have focused here in ultrasonic applications, in which chirp signals with specific bandwidth

and properties are required, but could be expanded for any application in which optimized APWP signals are required.

Regarding the digital pulsed nature of the resulting APWP signal, there is a substantial advantage if compared with analogue signal generators, as digital ones are faster, more reliable, smaller, programmable and with lower power requirements, what make them suitable for portable and/or autonomous systems and applications.

It can also be optimized for different environments, being it the propagation path, transducer transfer function, or reflectivity properties of the material to be excited, as the optimization process accounts for all of them. It is quite simple and takes just a few minutes for each optimization process, which is quite practical considering that this is only needed in the calibration stage of any experimental task.

As future works, the optimization algorithm, which is now by simple recursivity, could be developed to make it more efficient, although not really needed unless working with very long signals. On the other hand, it would be interesting if the shape of the spectrum could be also selected with some specific trend, for which the optimization rules should be adapted to the spectral shape desired.

REFERENCES

[1] C. H. Chen, *Ultrasonic and Advanced Methods for Nondestructive Testing and Material Characterization*. Singapore: World Scientific, 2007, doi: 10.1142/6327.

[2] A. S. Birks, R. E. Green, and P. McIntre, "Ultrasonic testing," in *Nondestructive Testing Handbook*. Columbus, OH, USA: American Society for Nondestructive Testing, 2007.

[3] J. David and N. Cheeke, *Fundamentals and Applications of Ultrasonic Waves*. Boca Raton, FL, USA, CRC Press, 2012, doi: 10.1201/b12260.

[4] R. J. Pyle, R. L. T. Bevan, R. R. Hughes, R. K. Rachev, A. A. S. Ali, and P. D. Wilcox, "Deep learning for ultrasonic crack characterization in NDE," *IEEE Trans. Ultrason., Ferroelectr., Freq. Control*, vol. 68, no. 5, pp. 1854–1865, May 2021, doi: 10.1109/TUFFC.2020.3045847.

[5] H.-D. Liang, J. A. Noble, and P. N. T. Wells, "Recent advances in biomedical ultrasonic imaging techniques," *Interface Focus*, vol. 1, no. 4, pp. 475–476, Jun. 2011, doi: 10.1098/rsfs.2011.0042.

[6] J. Ye and N. Toyama, "Benchmarking deep learning models for automatic ultrasonic imaging inspection," *IEEE Access*, vol. 9, pp. 36986–36994, 2021, doi: 10.1109/ACCESS.2021.3062860.

[7] Y. Lu and I. S. Ahn, "Comparison of time frequency analysis techniques for ultrasonic NDE signal," in *Proc. IEEE Int. Conf. Technol.*, May 2011, pp. 585–590, doi: 10.1109/EIT.2011.5978610.

[8] R. Raiutis, O. Tumys, R. Kažys, and L. Mažeika, "A comparative study of time-frequency analysis techniques in the case of signal processing for ultrasonic NDT," *Insight-Non-Destructive Test. Condition Monitor.*, vol. 50, no. 11, pp. 628–633, Nov. 2008, doi: 10.1784/insi.2008.50.11.628.

[9] G. Jacovitti and G. Scarano, "Discrete time techniques for time delay estimation," *IEEE Trans. Signal Process.*, vol. 41, no. 2, pp. 525–533, Feb. 1993, doi: 10.1109/78.193195.

[10] L. Svilainis, K. Lukoseviciute, and D. Liaukonis, "Reiterative deconvolution: New technique for time of flight estimation errors reduction in case of close proximity of two reflections," *Ultrasonics*, vol. 76, pp. 154–165, Apr. 2017, doi: 10.1016/j.ultras.2017.01.003.

[11] L. Svilainis, "Review on time delay estimate subsample interpolation in frequency domain," *IEEE Trans. Ultrason., Ferroelectr., Freq. Control*, vol. 66, no. 11, pp. 1691–1698, Nov. 2019, doi: 10.1109/TUFFC.2019.2930661.

[12] A. Aleksandrovas, A. Rodriguez, L. Svilainis, M. A. de la Casa, and A. Salazar, "Ultrasound-based density estimation of composites using water-air interface," *Elektronika Elektrotechnika*, vol. 22, no. 6, pp. 28–32, Dec. 2016, doi: 10.5755/j01.eie.22.6.17219.

[13] A. Rodríguez-Martínez, M. Á. de la Casa-Lillo, L. Svilainis, and T. E. G. Álvarez-Arenas, "Characterization of nanoparticles doped composites using ultrasound," *Ultrasonics*, vol. 83, pp. 68–79, Feb. 2018, doi: 10.1016/j.ultras.2017.06.017.

[14] A. Rodríguez, L. Svilainis, V. Dumbrava, A. Chaziachmetovas, and A. Salazar, "Automatic simultaneous measurement of phase velocity and thickness in composite plates using iterative deconvolution," *NDT E Int.*, vol. 66, pp. 117–127, Sep. 2014, doi: 10.1016/j.ndteint.2014.06.001.

[15] H. García-Martínez, E. Ávila-Navarro, G. Torregrosa-Penalva, A. Rodríguez-Martínez, C. Blanco-Angulo, and M. A. de la Casa-Lillo, "Low-cost additive manufacturing techniques applied to the design of planar microwave circuits by fused deposition modeling," *Polymers*, vol. 19, no. 2, p. 1496, Aug. 2020, doi: 10.3390/polym12091946.

[16] T. E. Gómez Álvarez-Arenas, "Simultaneous determination of the ultrasound velocity and the thickness of solid plates from the analysis of thickness resonances using air-coupled ultrasound," *Ultrasonics*, vol. 50, no. 2, pp. 104–109, Feb. 2010, doi: 10.1016/j.ultras.2009.09.009.

[17] A. Rodríguez, R. Miralles, I. Bosch, and L. Vergara, "New analysis and extensions of split-spectrum processing algorithms," *NDT E Int.*, vol. 45, no. 1, pp. 141–147, Jan. 2012, doi: 10.1016/j.ndteint.2011.10.001.

[18] A. Rodríguez, A. Salazar, and L. Vergara, "Analysis of split-spectrum algorithms in an automatic detection framework," *Signal Process.*, vol. 92, no. 9, pp. 2293–2307, Sep. 2012, doi: 10.1016/j.sigpro.2012.03.005.

[19] M. Pollakowski, H. Ermert, L. von Bernus, and T. Schmeidl, "The optimum bandwidth of chirp signals in ultrasonic applications," *Ultrasonic*, vol. 31, no. 6, pp. 417–420, Nov. 1993, doi: 10.1016/0041-624X(93)90049-6.

[20] F. Honarvar, H. Sheikhzadeh, M. Moles, and A. N. Sinclair, "Improving the time-resolution and signal-to-noise ratio of ultrasonic NDE signals," *Ultrasonics*, vol. 41, no. 9, pp. 755–763, 2004, doi: 10.1016/j.ultras.2003.09.004.

[21] M. L. Oelze, "Bandwidth and resolution enhancement through pulse compression," *IEEE Trans. Ultrason., Ferroelectr., Freq. Control*, vol. 54, no. 4, pp. 766–781, Apr. 2007, doi: 10.1109/TUFFC.2007.

[22] H. Huang and D. Paramo, "Broadband electrical impedance matching for piezoelectric ultrasound transducers," *IEEE Trans. Ultrason., Ferroelectr., Freq. Control*, vol. 58, no. 12, pp. 2699–2707, Dec. 2011, doi: 10.1109/TUFFC.2011.2132.

[23] T. Misaridis and J. A. Jensen, "Use of modulated excitation signals in medical ultrasound. Part II: Design and performance for medical imaging applications," *IEEE Trans. Ultrason., Ferroelectr., Freq. Control*, vol. 52, no. 2, pp. 192–207, Feb. 2005, doi: 10.1109/TUFFC.2005.1406546.

[24] T. Virolainen, J. Eskelinen, and E. Hägström, "Frequency domain low time-bandwidth product chirp synthesis for pulse compression side lobe reduction," in *Proc. IEEE Int. Ultrason. Symp.*, May 2009, pp. 1526–1528, doi: 10.1109/ULTSYM.2009.5441618.

[25] M. Zapf, B. F. Derouiche, and N. V. Ruiter, "Evaluation of chirp and binary code based excitation pulses for 3D USCT," in *Proc. IEEE Int. Ultrason. Symp.*, Sep. 2009, pp. 1996–1999, doi: 10.1109/ULTSYM.2009.5441916.

[26] C. Yoon, W. Lee, J. H. Chang, T.-K. Song, and Y. Yoo, "An efficient pulse compression method of chirp-coded excitation in medical ultrasound imaging," *IEEE Trans. Ultrason., Ferroelectr., Freq. Control*, vol. 60, no. 10, pp. 2225–2229, Oct. 2013, doi: 10.1109/TUFFC.2013.2815.

[27] D. Danial, M. Porat, and Z. Friedman, "On chirp excitation and compression for ultrasound imaging," in *Proc. IEEE Int. Conf. Sci. Electr. Eng. (ICSEE)*, Nov. 2016, pp. 1–5, doi: 10.1109/ICSEE.2016.7806106.

[28] S.-W. Huang and P.-C. Li, "Arbitrary waveform coded excitation using bipolar square wave pulsers in medical ultrasound," *IEEE Trans. Ultrason., Ferroelectr., Freq. Control*, vol. 53, no. 1, pp. 106–116, Jan. 2006, doi: 10.1109/TUFFC.2006.1588396.

[29] L. Svilainis and A. Aleksandrovas, "Application of arbitrary pulse width and position trains for the correlation sidelobes reduction for narrowband transducers," *Ultrasonics*, vol. 53, pp. 1344–1348, Sep. 2013, doi: 10.1016/j.ultras.2013.04.001.

[30] T. Folkestad and K. S. Mylvaganam, "Chirp excitation of ultrasonic probes and algorithm for filtering transit times in high-rangeability gas flow metering," *IEEE Trans. Ultrason., Ferroelectr., Freq. Control*, vol. 40, no. 3, pp. 193–215, May 1993, doi: 10.1109/58.216833.

[31] D. Chimura and R. S. Toh ans Motooka, "Spectrum compensation for time-reversal method on ultrasonic target detection using pulse compression," *IEEE Trans. Ultrason., Ferroelectr., Freq. Control*, vol. 54, no. 12, Dec. 2017, pp. 1874–1883, doi: 10.1109/TUFFC.2017.2748968.

[32] M. A. Benkhelifa, M. Gindre, J.-Y. Le Huerou, and W. Urbach, "Echography using correlation techniques: Choice of coding signal," *IEEE Trans. Ultrason., Ferroelectr., Freq. Control*, vol. 41, no. 5, pp. 579–587, Sep. 1994, doi: 10.1109/58.308492.

[33] L. Svilainis, S. Kitov, A. Rodríguez, L. Vergara, V. Dumbrava, and A. Chaziachmetovas, "Comparison of spread spectrum and pulse signal excitation for split spectrum techniques composite imaging," *IOP Conf., Mater. Sci. Eng.*, vol. 42, Oct. 2012, Art. no. 012007, doi: 10.1088/1757-899X/42/1/012007.

[34] A. Rodriguez, A. Salazar, L. Vergara, F. J. Gimeno-Blanes, L. Svilainis, V. Dumbrava, S. Kitov, and A. Chaziachmetovas, "Split spectrum processing applications for new composite materials imaging," in *Proc. IEEE Int. Ultrason. Symp.*, Oct. 2012, pp. 1473–1476, doi: 10.1109/ULTSYM.2012.0368.

[35] D. Hutchins, P. Burrascano, L. Davis, S. Laureti, and M. Ricci, "Coded waveforms for optimised air-coupled ultrasonic nondestructive evaluation," *Ultrasonics*, vol. 54, no. 7, pp. 1745–1759, 2014, doi: 10.1016/j.ultras.2014.03.007.

[36] F. J. Álvarez, Á. Hernández, J. Ureña, M. Mazo, J. J. García, J. A. Jiménez, and A. Jiménez, "Real-time implementation of an efficient correlator for complementary sets of four sequences applied to ultrasonic pulse compression systems," *Microprocessors Microsyst.*, vol. 30, no. 1, pp. 43–51, Feb. 2006, doi: 10.1016/j.micpro.2005.04.003.

[37] L. Svilainis, A. Aleksandrovas, K. Lukoseviciute, and V. Eidukynas, "Investigation of the time of flight estimation errors induced by neighboring signals," in *Proc. IEEE Int. Intell. Data Acquisition Adv. Comput. Syst.*, May 2013, pp. 413–418, doi: 10.1109/IDAACS.2013.6662718.

[38] A. Misaridis, "Ultrasound imaging using coded signals," Ph.D. dissertation, Dept. Electr. Eng., Tech. Univ. Denmark, Lyngby, Denmark, 2001. [Online]. Available: https://orbit.dtu.dk/en/publications/ultrasound-imaging-using-coded-signals

[39] D. Chimura, R. Toh, and S. Motooka, "Ultrasonic direction measurement method using sensitivity compensated transmitting signal and pulse compression," *Phys. Proc.*, vol. 70, pp. 476–479, Jan. 2015, doi: 10.1016/j.phpro.2015.08.289.

[40] R. Toh and S. Motooka, "Target ranging using ultrasonic sensitivity compensated signal and pulse compression," *Jpn. J. Appl. Phys.*, vol. 48, pp. 7–9, Oct. 2009, doi: 10.3135/jmasj.38.61.

[41] L. Svilainis, V. Dumbrava, S. Kitov, A. Aleksandrovas, A. Chaziachmetovas, V. Eidukynas, D. Kybartas, and K. Lukoseviciute, "Acquisition system for the arbitrary pulse width and position signals application in ultrasound," *Sensor Lett.*, vol. 12, no. 9, pp. 1399–1407, Sep. 2014, doi: 10.1166/sl.2014.3329.

[42] L. Svilainis, V. Dumbrava, S. Kitov, A. Aleksandrovas, P. Tervydis, and D. Liaukonis, "Electronics for ultrasonic imaging system," *Elektronika Elektrotechn.*, vol. 20, no. 7, pp. 51–56, Sep. 2014, doi: 10.5755/j01.eee.20.7.8024.

[43] L. Svilainis, V. Dumbrava, A. Chaziachmetovas, and A. Aleksandrovas, "Pulser for arbitrary width and position square pulse trains generation," in *Proc. IEEE Int. Ultrason. Symp.*, Oct. 2012, pp. 1–4, doi: 10.1109/ULTSYM.2012.0438.

[44] A. Chaziachmetovas, L. Svilainis, D. Kybartas, A. Aleksandrovas, and D. Liaukonis, "Evaluation of material nonlinearities using rectangular pulse trains for excitation," *Phys. Proc.*, vol. 70, pp. 582–585, 2015, doi: 10.1016/j.phpro.2015.08.026.

[45] L. Svilainis, A. Rodriguez-Martinez, A. Chaziachmetovas, and A. Aleksandrovas, "Ultrasound transmission spectral compensation using arbitrary position and width pulse sets," *IEEE Trans. Instrum. Meas.*, vol. 67, no. 8, pp. 1778–1785, Aug. 2018, doi: 10.1109/TIM.2018.2809838.

[46] I. Amir, N. M. Bilgutay, and V. L. Newhouse, "Analysis and comparison of some frequency compound in algorithms for the reduction of ultrasonic clutter," *IEEE Trans. Ultrason., Ferroelectr., Freq. Control*, vol. UFFC-33, no. 4, pp. 402–411, Jul. 1986, doi: 10.1109/T-UFFC.1986.26848.

[47] B. Zhang, X. Ding, and W. Zhu, "An asymmetric split-spectrum method for estimating the ionospheric artifacts in insar data," in *Proc. IEEE Int. Geosci. Remote Sens. Symp.*, Jul. 2018, pp. 517–520, doi: 10.1109/IGARSS.2018.8518936.

[48] Y. Jia, O. Tan, J. Tokayer, B. Potsaid, Y. Wang, and J. Liu, "Split-spectrum amplitude-decorrelation angiography with optical coherence tomography," *Opt. Exp.*, vol. 20, no. 4, pp. 4710–4725, 2012, doi: 10.1364/OE.20.004710.

[49] M. Furuya, T. Suzuki, J. Maeda, and K. Heki, "Midlatitude sporadic-E episodes viewed by L-band split-spectrum InSAR," *Earth, Planets Space*, vol. 69, no. 1, pp. 1–10, Dec. 2017, doi: 10.1186/s40623-017-0764-6.

A. RODRÍGUEZ-MARTÍNEZ (Senior Member, IEEE) received the B.E. degree in telecommunications from the University of Vigo, Spain, in 1998, and the Ph.D. degree in telecommunications from the Polytechnic University of Valencia, Spain, in 2011.

He is currently an Associate Professor with the Department of Communications Engineering, University Miguel Hernandez of Elche, Elche, Spain. His research interests include time-to-frequency analysis, ultrasonic signals processing, for nondestructive materials characterization, and for biomedical signal processing.

L. SVILAINIS (Senior Member, IEEE) received the Ph.D. degree from the Kaunas University of Technology, Lithuania, in 1996.

Since 2009, he is currently a full-time Professor with the Department of Electronics Engineering, Kaunas University of Technology. His current research interests include ultrasound electronics and signal processing, large scale LED video displays, electromagnetic compatibility, and EMI protection of electronic systems.

M. A. DE LA CASA-LILLO received the bachelor's degree in chemistry from the University of Granada, Spain, in 1994, and the Ph.D. degree in chemistry (materials science program) from the University of Alicante, Spain, in 1999.

He is currently a Full Professor with the Department of Materials Science, Bioengineering Institute, University Miguel Hernandez of Elche, Elche, Spain. His current research interests include materials characterization, ultrasonic systems for non-destructive testing, and for biomedical and health applications.

T. G. ALVAREZ-ARENAS received the Ph.D. degree in physics from the Complutense University of Madrid.

In 1996, he joined as a Postdoctoral Researcher with the Center for Ultrasonic Engineering, Strathclyde University, Glasgow, U.K. In 2000, he joined the Institute of Acoustics, CSIC, and then the Institute of Physical and Information Technologies, ITEFI-CSIC, in 2013. Since 2014, he has been the Head of the Sensors and Ultrasonic Technologies Department, ITEFI-CSIC. He is currently a Scientist with Spanish National Research Council (CSIC). His research interests include design, optimization and fabrication of piezoelectric transducers, piezoelectric and ferroelectric materials, ultrasonic materials characterization, new materials for ultrasonic applications, solution of inverse and hard optimization problems and applications of ultrasonic techniques in NDT, medical diagnosis, food quality, industrial control, and agriculture sensing.

A. ALEKSANDROVAS received the B.S. and M.S. degrees in electronics engineering and the Ph.D. degree in electrical and electronic engineering from the Kaunas University of Technology, Lithuania, in 2011, 2013, and 2018, respectively.

His current research interests include ultrasound electronics, ultrasonic data acquisition, embedded software development, ultrasonic signals processing, and time of flight estimation.

A. SALAZAR (Member, IEEE) received the B.S. degree in computer science engineering, in 2004, and the Ph.D. degree and the M.S. degree in artificial intelligence and pattern recognition from the Universitat Politècnica de València, in 2011 and 2020, respectively.

He works with the Institute of Telecommunications and Multimedia Applications, Universitat Politècnica de València. His research interests include statistical signal processing, machine learning, decision fusion, pattern recognition, and graph signal processing. The methods in which he has researched have been applied in several fields, such as brain signal dynamic modeling, material non-destructive testing, and credit card fraud detection.

● ● ●

A. CHAZIACHMETOVAS received the B.S. and M.S. degrees in electronics engineering from the Kaunas University of Technology, Lithuania, in 2000 and 2002, respectively, and the Ph.D. degree in metrology and measurements, in 2007.

From 2007 to 2009, he was an Assistant and a Researcher with the Department of Signal Processing. Since 2009, he is an Associate Professor with the Department of Electronics Engineering, Kaunas University of Technology. His current research interests include ultrasonic measurements, ultrasound electronics, high voltage pulsers, software development, embedded systems, time of flight estimation, and laser ultrasound.